Available online at www.sciencedirect.com
ScienceDirect
Journal of Sound and Vibration 310 (2008) 845–854
JOURNAL OF SOUND AND VIBRATION
www.elsevier.com/locate/jsvi

An estimation method for acoustic scattering from convex bodies

Vitaliy P. Chumachenko, Alexander V. Krapyvny*, Yaroslav V. Chumachenko

Zaporizhzhya National Technical University, 64 Zhukovsky Str., Zaporizhzhya, 69063, Ukraine

Received 30 March 2007; received in revised form 15 July 2007; accepted 7 August 2007
Available online 18 September 2007

Abstract

The problem of plane-wave scattering from a convex body with a soft, rigid or impedance surface is considered. In common with physical optics (PO), the proposed approach exploits the locality property of short-wave scattering. However, in contrast to the PO approximation it considers the curvature of the target and the shadow-side fields. The theory is based on the assumption that each element of integration in the Kirchhoff integral is a patch of a circular cylinder perpendicular to the plane of incidence. Extensive comparisons with exact solutions for spheres of different sizes with constant surface impedances have shown that the approach is more accurate than PO and keeps the PO-comparable simplicity. Although the method is strictly valid for high frequencies, it gives good quantitative results down to resonant frequency range. The approach was also tested on the problem of scattering from a rigid prolate spheroid. An example of application of the technique to a prolate spheroid with a varying surface impedance is presented.

1. Introduction

The scattering of a scalar wave by an obstacle is a fundamental problem of acoustics. It has attracted considerable attention of investigators for many years. Exact analytical solutions to the scalar wave equation exist only for a few geometries for which the separation of variables is possible [1]. For more complex shapes, approximate analytical and numerical approaches have been developed. Some of the previous work is found in Refs. [2–9]. Each of such techniques has an application domain, which is restricted in one or more by configuration of the boundary, wave size of the scatterer, types of boundary conditions, the incidence or the response direction, and the efficiency of numerical implementation.

At the resonant frequency range, the exact formulations (as, for example, the Helmholtz integral equation [3,6]) are mainly used. With the help of certain procedures they are usually approximated by a system of linear algebraic equations. At that, the number of unknowns, which dictates the matrix size of the system, increases with increasing wavenumber. For large body problems (relative to a wavelength) this matrix becomes very large. Therefore, for shorter waves the technique becomes increasingly inefficient owing to inadequacy of

*Corresponding author. Tel.: +380 66 720 4770.
E-mail addresses: chumac@zntu.edu.ua (V.P. Chumachenko), akrapyvn@zntu.edu.ua (A.V. Krapyvny), fiveua@yandex.ru (Y.V. Chumachenko).

0022-460X/$ - see front matter © 2007 Elsevier Ltd. All rights reserved.
doi:10.1016/j.jsv.2007.08.003

computer resources. At high frequencies, one of possible alternatives is the method of physical optics (PO) (Kirchhoff approximation) [4,10] which is frequently used to derive the wave scattered from an arbitrary target. This wave is obtained as an integral over the surface elements, each of which has a reflection coefficient equal to that of an infinite plane surface. Over the shadow part of the body, the field is taken to be zero. The approach is simple and extremely efficient, since it requires no matrix solution. However, it is suitable for treating only large objects with smooth surfaces. In addition, the PO prediction deteriorates as the scattering direction moves further from the specular direction.

Recently a new approach was proposed to approximately solve scattering problems for soft and rigid convex cylinders [11]. Similarly to PO, this technique exploits the locality property of short-wave scattering and yields an analytical expression for the surface pressure and particle velocities. However, in contrast to PO approximation it takes into account the curvature of the surface and does not suppose that the field vanishes in the shadow region. By using this method, the result is that at the PO-comparable simplicity the accuracy of the prediction in the non-specular direction (especially in forward direction) can be improved appreciably. In Ref. [12], the technique was extended to the case of an impedance cylinder. In this paper, the approach is generalized to three dimensions to handle a convex target bounded by a soft, rigid or impedance surface. The analysis is based on the assumption that each element of integration in the Kirchhoff integral is a patch of an infinite circular cylinder perpendicular to the plane of incidence passing through the point of integration.

2. Theory

Let (x, y, z) and (r, θ, ϕ) be basic Cartesian and spherical coordinate systems and S be a smooth boundary of a convex body which possesses (in general) a surface impedance Z. The incident acoustic plane wave is described as

$$p_i = \mathrm{e}^{-\mathrm{i}\mathbf{k_i}\cdot\mathbf{r}}, \tag{1}$$

where $\mathbf{k_i} = k\hat{k}_i$, $k = \omega/c = 2\pi/\lambda$, ω is the angular frequency, c the sound speed and λ the wave length in the medium, and $\mathbf{r} = x\hat{x} + y\hat{y} + z\hat{z}$. The symbols with '$\hat{}$' denote unit vectors. The harmonic time dependence $\mathrm{e}^{\mathrm{i}\omega t}$ is assumed and suppressed. The wave comes from a source with angular data θ_i and ϕ_i.

The total pressure

$$p = p_i + p_s \tag{2}$$

satisfies the Helmholz equation outside the scatterer and the impedance boundary conditions

$$\frac{\partial p}{\partial n} - \mathrm{i}k\chi p = 0 \tag{3}$$

on its surface. Here $\mathbf{n}$ is the outward normal to the surface S, $\chi = Z_0/Z$, $Z_0 = c\rho_0$ is the characteristic impedance and ρ_0 the mass density of the medium. The value $\chi = 0$ corresponds to a rigid target. For a soft body, we have $\chi = \infty$ and

$$p = 0 \tag{4}$$

on its surface.

The scattered wave p_s must satisfy the Sommerfeld radiation condition. According to the Kirchhoff integral theorem, at far field it can be written in the form

$$p_s(M) \approx f(\theta_M, \phi_M)\frac{\mathrm{e}^{-\mathrm{i}kr_M}}{r_M}. \tag{5}$$

Here θ_M and ϕ_M are angular coordinates of an observation point M with the position vector $\mathbf{r}_M$ and $f(\theta_M, \phi_M)$ is the scattering amplitude, which can be evaluated from the surface integration as

$$f(\theta_M, \phi_M) = -\frac{1}{4\pi}\int\int_S \mathrm{e}^{\mathrm{i}kr_P\cos\psi}\left[\frac{\partial p(P)}{\partial n} - \mathrm{i}kp(P)\cos\alpha\right]\mathrm{d}S_P. \tag{6}$$

In formula (6), $\mathbf{r}_P$ is the position vector of a point P on S, ψ the angle between $\mathbf{r}_M$ and $\mathbf{r}_P$, and α is that between $\mathbf{n}_P$ and $\mathbf{r}_M$. In view of Eq. (3), the last expression can be rewritten as

$$f(\theta_M, \phi_M) = -\frac{\mathrm{i}k}{4\pi} \int\int_S \mathrm{e}^{\mathrm{i}kr_P \cos\psi} p(P)[\chi(P) - \cos\alpha]\,\mathrm{d}S_P. \tag{7}$$

For a soft target, formula (6) is reduced to

$$f(\theta_M, \phi_M) = \frac{\mathrm{i}kZ_0}{4\pi} \int\int_S \mathrm{e}^{\mathrm{i}kr_P \cos\psi} v_n(P)\,\mathrm{d}S_P, \tag{8}$$

where

$$v_n(P) = \frac{\mathrm{i}}{kZ_0} \frac{\partial p(P)}{\partial n} \tag{9}$$

is the normal component of the particle velocity at P. As usual, the scattering cross section is defined as

$$\sigma = 4\pi|f|^2. \tag{10}$$

Using PO approximation, we can readily estimate $p(P)$ in Eq. (7) as

$$p(P) = \begin{cases} p_i(P) \dfrac{2\cos\gamma}{\cos\gamma + \chi(P)} & \text{for } \gamma \leqslant \dfrac{\pi}{2}, \\ 0 & \text{for } \gamma > \dfrac{\pi}{2} \end{cases} \tag{11}$$

and $v_n(P)$ in Eq. (8) as

$$v_n(P) = \begin{cases} -p_i(P) \dfrac{2\cos\gamma}{Z_0} & \text{for } \gamma \leqslant \dfrac{\pi}{2}, \\ 0 & \text{for } \gamma > \dfrac{\pi}{2}. \end{cases} \tag{12}$$

Here, γ is the angle of incidence at P, i.e. the angle between $\mathbf{n}_P$ and $(-\mathbf{k}_i)$.

The cross section of the target by the plane of incidence, passing through the point P, is shown in Fig. 1. For visualization, the origin O of the basic coordinate system and an observation point M are given at the same plane. The point C indicates the centre of curvature at P for the contour of the section. The dashed line

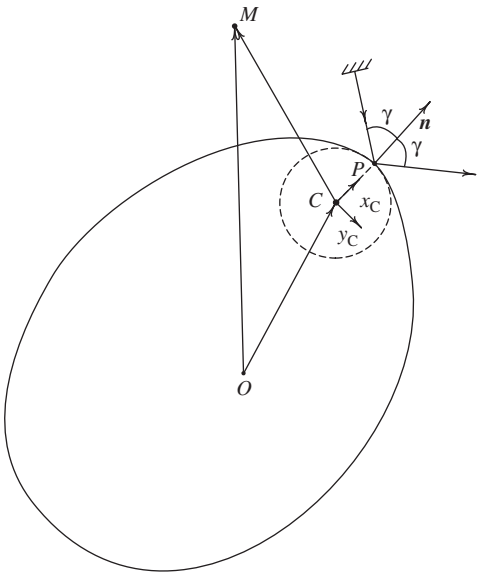

Fig. 1. Geometry of the problem.

presents the respective circle of curvature. In order to improve the estimates for $p(P)$ and $v_n(P)$, we consider the vicinity of the point P on S as a patch of a cylinder, which is perpendicular to the above section and has the circle of curvature as directrix.

Let (x_C, y_C, z_C) be a Cartesian coordinate system with $\hat{x}_C = \mathbf{n}_P$ and z_C along the axis of the cylinder, and (ρ, φ, z_C) a cylindrical coordinate system with $\varphi = 0$ at $y_C = 0$ and $x_C > 0$. The orientation of the systems we choose in such a way that φ increases when moving from the insonified region toward the shadow part of the scatterer. Then

$$\hat{k}_i = -\cos\gamma\hat{x}_C + \sin\gamma\hat{y}_C, \tag{13}$$

$$\overline{CM} = \rho\,\cos\varphi\hat{x}_C + \rho\,\sin\varphi\hat{y}_C + z_C\hat{z}_C \tag{14}$$

and

$$p_i(M) = \mathrm{e}^{-\mathrm{i}\mathbf{k}_\mathbf{i}\cdot\mathbf{r}_M} = \mathrm{e}^{-\mathrm{i}\mathbf{k}_\mathbf{i}\cdot\overline{OC}}\mathrm{e}^{-\mathrm{i}\mathbf{k}_\mathbf{i}\cdot\overline{CM}} = A\mathrm{e}^{\mathrm{i}k\rho(\cos\varphi\cos\gamma - \sin\varphi\sin\gamma)} = A\mathrm{e}^{\mathrm{i}k\rho\,\cos(\varphi+\gamma)}, \tag{15}$$

where A is a constant for a fixed P. By using expansion of $\cos(\varphi+\gamma)$ in powers of φ, we obtain on the scattering surface near P:

$$p_i(M) = A\mathrm{e}^{\mathrm{i}kR(\cos\gamma - \varphi\sin\gamma + \cdots)} \approx A\mathrm{e}^{\mathrm{i}kR(\cos\gamma - \varphi\sin\gamma)}, \tag{16}$$

where $R = |\overline{CP}|$ is the radius of curvature.

In the neighbourhood of P, by separating variables in the cylindrical coordinates introduced, we represent p_s in the form of an outgoing wave

$$p_s = (K\mathrm{e}^{\mathrm{i}\mu\varphi} + L\mathrm{e}^{-\mathrm{i}\mu\varphi})(N\mathrm{e}^{\mathrm{i}vz_C} + T\mathrm{e}^{-\mathrm{i}vz_C})H_\mu^{(2)}(\sqrt{k^2 - v^2}\rho). \tag{17}$$

Here, K, L, N, T and μ, v are constants, $H_\mu^{(2)}$ is the Hankel function. Next, we assume that over the above patch the functional dependence of p_s coincides with that of p_i within to a constant factor just as in the case of a plane reflecting surface. Comparing Eq. (17) at $\rho = R$ and Eq. (16), we find that under this assumption p_s must be independent of z_C (i.e. $v = 0$), $K = 0$,

$$\mu = kR\,\sin\gamma \tag{18}$$

and

$$p_s = BH_\mu^{(2)}(k\rho)\mathrm{e}^{-\mathrm{i}\mu\varphi}, \tag{19}$$

with $B = L(N + T)$. The constant B is found from the boundary condition (3) imposed at the point P. Taking into account equalities (2) and $\partial\cdot/\partial n = \partial\cdot/\partial\rho$, we obtain

$$B = \mathrm{i}\frac{p_i(P)[\chi(P) - \cos\gamma]}{H_\mu^{(2)}(kR)[\sin\gamma - H_{\mu+1}^{(2)}(kR)/H_\mu^{(2)}(kR) - \mathrm{i}\chi(P)]}. \tag{20}$$

Substituting Eq. (20) in Eq. (19) and Eq. (19) in Eq. (2), we get

$$p(P) = p_i(P)\left[1 + \mathrm{i}\frac{\chi(P) - \cos\gamma}{\sin\gamma - H_{\mu+1}^{(2)}(kR)/H_\mu^{(2)}(kR) - \mathrm{i}\chi(P)}\right], \tag{21}$$

where $\gamma \in [0, \pi]$.

In the case of a soft target, we similarly arrive at

$$B = -p_i(P)/H_\mu^{(2)}(kR) \tag{22}$$

and

$$v_n(P) = -\frac{p_i(P)}{Z_0}\left[\cos\gamma + \mathrm{i}\,\sin\gamma - \mathrm{i}\frac{H_{\mu+1}^{(2)}(kR)}{H_\mu^{(2)}(kR)}\right], \tag{23}$$

with the same μ and $\gamma \in [0, \pi]$.

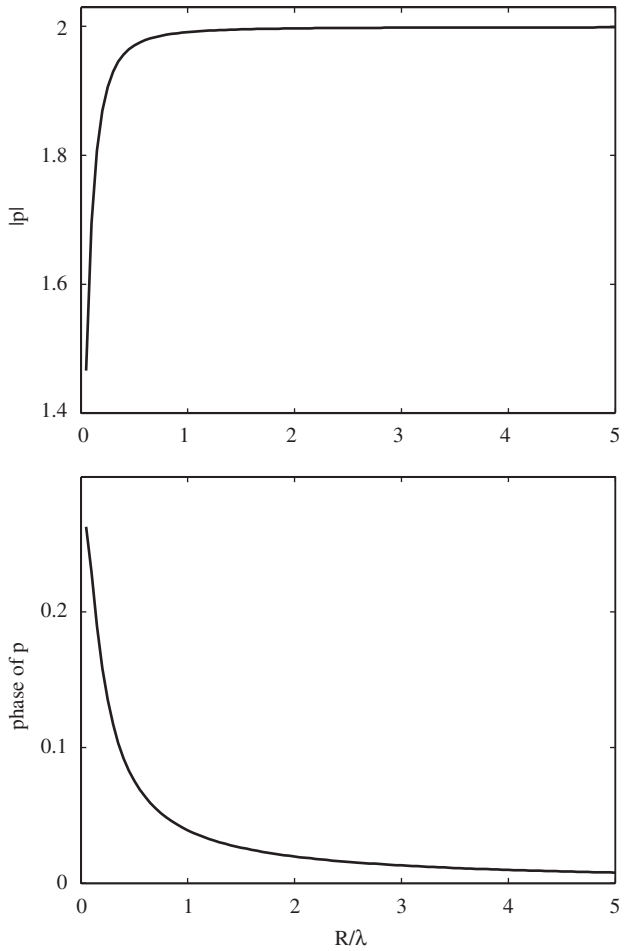

Fig. 2. Total surface pressure for a rigid surface as a function of R/λ at $\gamma = 0$ and $p_i(P) = 1$.

Notice that the plane of incidence (and consequently R) is not defined at two points with $\gamma = 0$ and π. However, at $\mu = 0$, $p(P)$ in Eq. (21) and $v_n(P)$ in Eq. (23) weakly depend on R/λ when $R/\lambda > 0.5$. Fig. 2 illustrates this case for a rigid surface. Therefore, as R we can take, for example, the average of possible values of radius of curvature at P. Practically, this choice does not affect the scattering amplitude since its values are found from the surface integration.

Let us also show that the PO formulas (11) and (12) are limiting cases of Eqs. (21) and (23) as $R \to \infty$. To this end, we derive the asymptotic form of the expression

$$\sin\gamma - \frac{H_{\mu+1}^{(2)}(kR)}{H_{\mu}^{(2)}(kR)} = \frac{H_{\mu}^{(2)\prime(kR)}}{H_{\mu}^{(2)}(kR)}, \tag{24}$$

which is a component part of the above equations. Let $\cos\beta = \sin\gamma$ with $0 < \beta < \pi/2$. Then

$$\beta = \begin{cases} \dfrac{\pi}{2} - \gamma & \text{for } \gamma < \dfrac{\pi}{2}, \\ \gamma - \dfrac{\pi}{2} & \text{for } \dfrac{\pi}{2} < \gamma < \pi. \end{cases} \tag{25}$$

If we use the dominant terms of the known [13] asymptotic expansions, we obtain as $R \to \infty$

$$H_{\mu}^{(2)}(kR) = H_{\mu}^{(2)}(\mu/\cos\beta) \sim \sqrt{\frac{2}{\pi\mu\tan\beta}}\, e^{-i[\mu(\tan\beta-\beta)-\pi/4]}, \tag{26}$$

$$H_{\mu}^{(2)\prime}(kR) = H_{\mu}^{(2)\prime}(\mu/\cos\beta) \sim -i\sqrt{\frac{\sin 2\beta}{\pi\mu}}\, e^{-i[\mu(\tan\beta-\beta)-\pi/4]}. \tag{27}$$

Now, in view of Eqs. (25)–(27), we have

$$\frac{H_{\mu}^{(2)\prime}(kR)}{H_{\mu}^{(2)}(kR)} \sim -i\sqrt{\frac{1}{2}\sin 2\beta\tan\beta} = -i\sin\beta = \begin{cases} -i\cos\gamma & \text{for } 0<\gamma<\dfrac{\pi}{2}, \\ i\cos\gamma & \text{for } \dfrac{\pi}{2}<\gamma<\pi. \end{cases} \tag{28}$$

Substituting Eq. (28) into Eqs. (24), (21) and (23), we arrive just at Eqs. (11) and (12). For the angles $\gamma = 0$, $\pi/2$ and π, the limiting cases can be also easily verified using other [13] asymptotic representations of the Hankel function.

3. Numerical results

The results plotted in this section were generated using Eqs. (7)–(12), (21) and (23) to illustrate predictions and demonstrate the accuracy of the approach. Figs. 3 and 4 present data for a target with sufficiently small (for a high-frequency technique) wave dimensions. In Fig. 3, the pressure and the velocity calculated on the surface of a sphere of radius $R = \lambda$ are compared with those obtained from the PO approximation and with a numerical implementation of the exact analytical solution [1]. The origin of the basic coordinate system is at the centre of the sphere and $\theta_i = 0$. It is seen, that p and v_n computed with the aid of this technique do not vanish on the shadow part of the target. The data obtained are much better than the PO prediction qualitatively and quantitatively. Fig. 4 shows the respective angular dependencies for the scattering magnitude. In the non-specular directions, the improvement is obvious.

Fig. 5 presents dependencies on R/λ of the relative mean-square error

$$\delta = \sqrt{\int_0^{\pi} |f - f_e|^2 \, d\theta_M} \Big/ \sqrt{\int_0^{\pi} |f_e|^2 \, d\theta_M}, \tag{29}$$

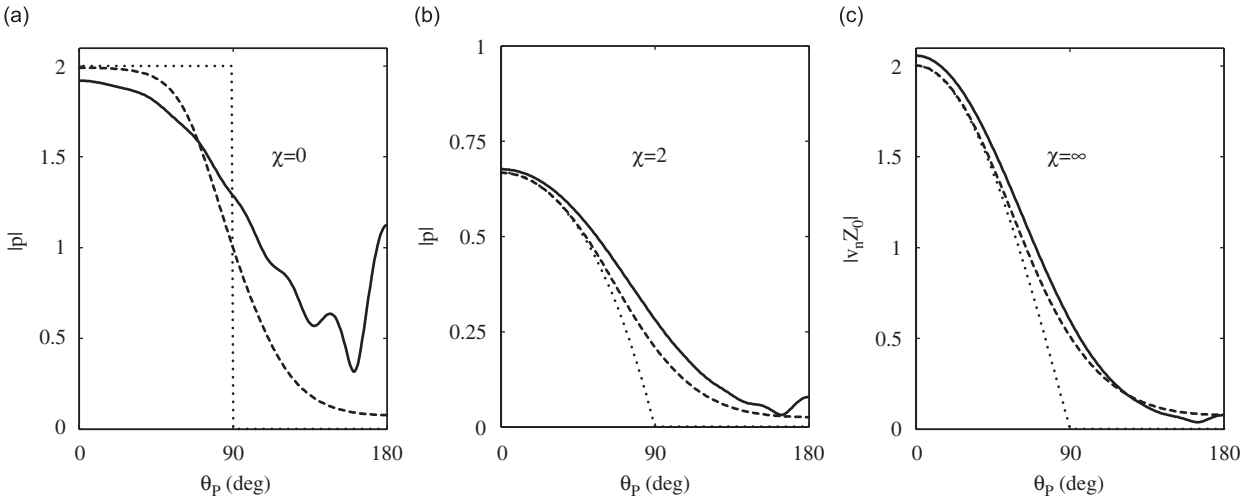

Fig. 3. The (a, b) total surface pressure and (c) surface velocity for (a) rigid, (b) impedance and (c) soft spheres at $R/\lambda = 1$ (solid lines: exact; dotted lines: PO; dashed lines: this technique).

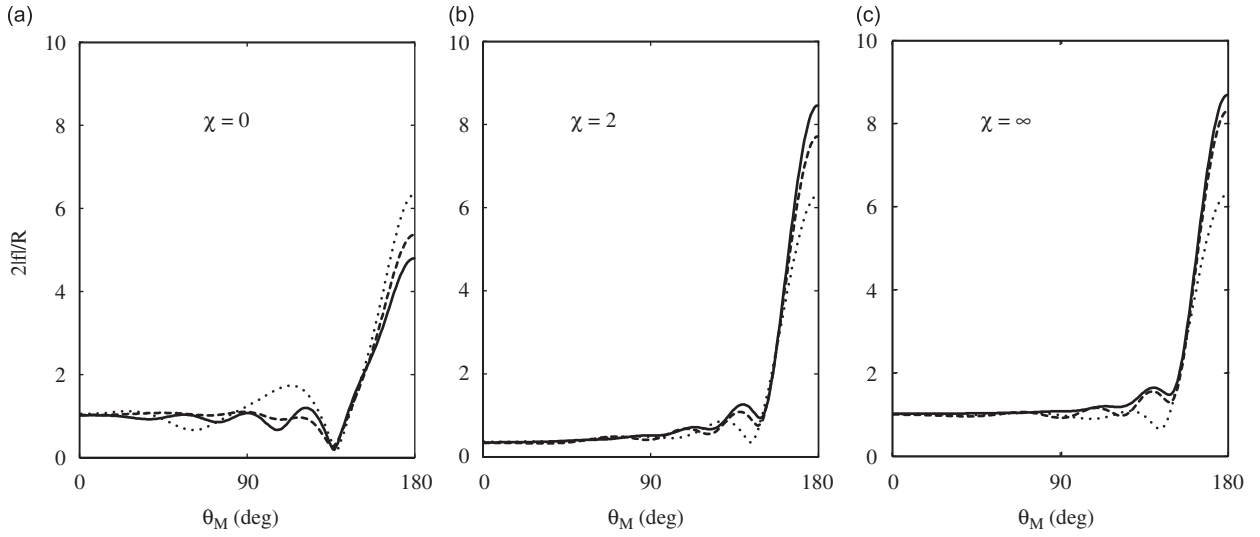

Fig. 4. Normalized form function for (a) rigid, (b) impedance and (c) soft spheres at $R/\lambda = 1$ (solid lines: exact; dotted lines: PO; dashed lines: this technique).

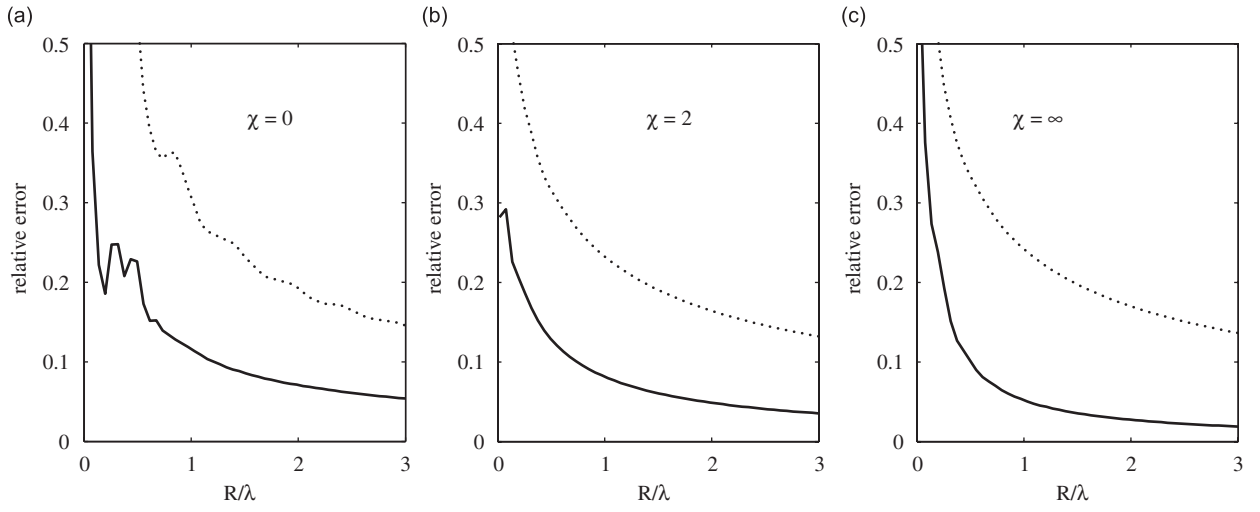

Fig. 5. Relative mean-square error δ for (a) rigid, (b) impedance and (c) soft spheres (solid lines: this technique; dotted lines: PO).

where f_e is the exact value of f, for a rigid, impedance and soft sphere. They estimate the accuracy of approximations for the whole interval $[0, \pi]$. In all the cases, the implementation of this formulation diminishes the error considerably and allows obtaining quantitatively adequate predictions up to resonant frequency range. Nevertheless, it is worth to note that R/λ should be at least greater than one for a rigid target to achieve the error, which is less than 10%.

In Fig. 6, we plot the normalized backward and forward cross section as a function of R/λ. Again, the results from the present method agree with the exact solution better than the PO approximation (especially in forward direction).

Now, let us consider a prolate spheroid whose axis of symmetry corresponds to the z-axis. The origin of the coordinate system is at the centre of the target and $\phi_i = 0$. The semi-major axis is b and semi-mine axis is a. The reduced target strength is defined as $\mathrm{RTS} = 20 \log |f/(2b)|$.

Fig. 7 shows comparisons of the computed predictions with the results obtained using the Fourier matching method (FMM) for a rigid prolate spheroid at broadside and end-on incidences. The FMM curves were taken from [9] and logarithmic scale on the horizontal axes was replaced by the linear one. It is evident that the

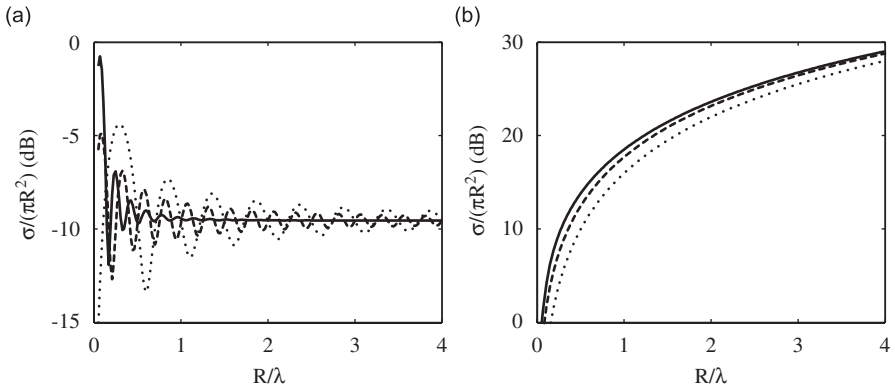

Fig. 6. Normalized cross section for (a) backward and (b) forward scattering spheres at $\chi = 2$ (solid lines: exact; dotted lines: PO; dashed lines: this technique).

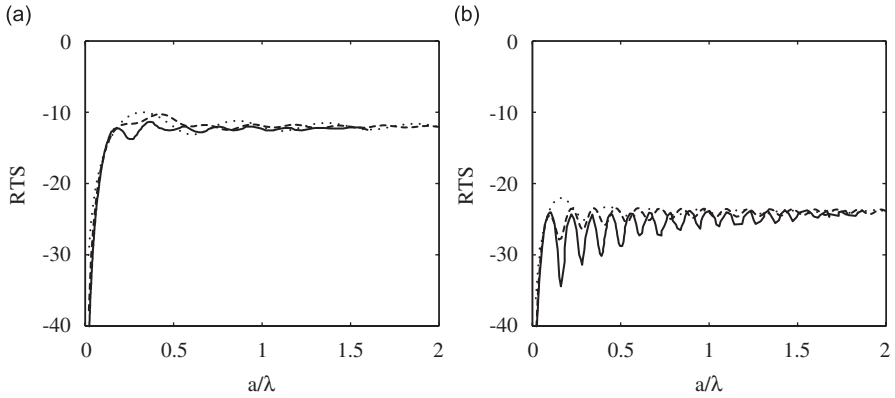

Fig. 7. Reduced target strength of a backward scattering prolate spheroid for aspect ratio of 2:1 at (a) $\theta_i = 90^\circ$ and (b) $\theta_i = 0^\circ$ (solid lines: results from [9]; dotted lines: PO; dashed lines: this technique).

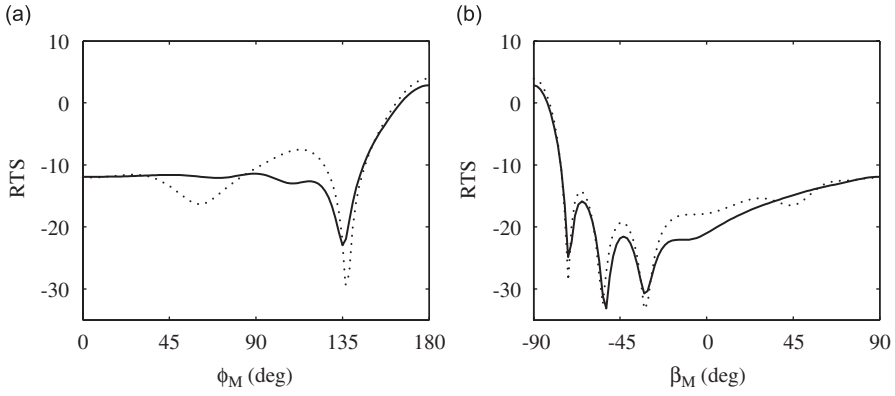

Fig. 8. Angular dependencies of the reduced target strength of a rigid prolate spheroid at the planes (a) $z = 0$ and (b) $y = 0$ for $a/\lambda = 1$, $\theta_i = 90^\circ$ and aspect ratio of 2:1. Tilt angle $\beta_M = \theta_M$ at $\phi_M = 0^\circ$ and $\beta_M = -\theta_M$ at $\phi_M = 180^\circ$ (solid lines: this technique; dotted lines: PO).

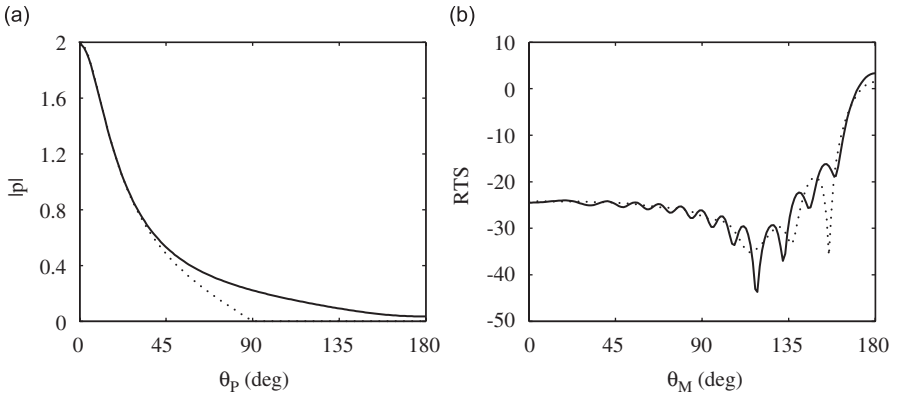

Fig. 9. The (a) total surface pressure and (b) reduced target strength of a prolate spheroid at $a/\lambda = 1.5$, $\theta_i = 0^\circ$ and $\chi = 1 - \cos\gamma$ for aspect ratio of 2:1 (solid lines: this technique; dotted lines: PO).

estimates of RTS found by this technique tend to the known solutions as a/λ increases. It should be also noted that at $a/\lambda < 2$ minimum radius of curvature of the considered spheroid is less than λ.

Next two figures present examples of application of the developed technique to estimating bistatic far-field patterns. Fig. 8 shows the bistatic scattering from the same rigid spheroid. In Fig. 9, we consider a prolate spheroid with variable surface impedance. Functional dependence $\chi = 1 - \cos\gamma$ implements the passage from the rigid surface on the insonified part of the target to the case of $\chi = 2$ in the shadow region. For comparison, the PO predictions are also given.

4. Conclusions

This paper presents a computationally easy approach to solve approximately high-frequency scattering problems for 3D convex obstacles bounded by soft, rigid or impedance surfaces. Sample results, which validate the theory and demonstrate its capabilities, are given. The approach is more accurate than the PO approximation and keeps the PO-comparable simplicity. It yields quantitatively adequate results up to resonant frequencies. The improvement in the prediction is especially considerable for the forward scattering. There is a good potential for further development of this technique including scattering by fluid bodies and elastic solids.

Acknowledgements

The authors would like to thank the reviewers for useful comments and suggestions.

References

[1] P.M. Morse, H. Feshbach, *Methods of Theoretical Physics*, McGraw-Hill, Boston, 1953.
[2] V.K. Varadan, V.V. Varadan, Computation of rigid body scattering by prolate spheroids, *Journal of the Acoustical Society of America* 71 (1982) 22–25.
[3] W. Tobocman, Calculation of acoustic wave scattering by means of the Helmholz integral equation. I, *Journal of the Acoustical Society of America* 76 (1984) 599–607.
[4] G.C. Gaunaurd, Sonar cross sections of bodies partially insonified by finite sound beams, *IEEE Journal of Ocean Engineering* OE-10 (1985) 213–230.
[5] G.A. Kriegsmann, T. Moor, An application of the on-surface radiation condition to the scattering of acoustic waves by a reactively loaded sphere, *Wave Motion* 10 (1988) 277–284.
[6] D.T.I. Francis, A gradient formulation for acoustic radiation and scattering, *Journal of the Acoustical Society of America* 93 (1993) 1700–1709.

[7] C. Partridge, E.R. Smith, Acoustic scattering from bodies: range of validity of the deformed cylinder method, *Journal of the Acoustical Society of America* 97 (1995) 784–795.
[8] Z. Ye, E. Hoskinson, R. Dewey, L. Ding, D.M. Farmer, A method for acoustic scattering by slender bodies. I. Theory and verification, *Journal of the Acoustical Society of America* 102 (1997) 1964–1976.
[9] B.B. Reeder, T.K. Stanton, Acoustic scattering by axisymmetric finite-length bodies: an extension of a two-dimensional conformal mapping method, *Journal of the Acoustical Society of America* 116 (2004) 729–746.
[10] E.F. Knott, J.F. Shaeffer, M.T. Tuley, *Radar Cross Section*, Artech House, Norwood, 1993.
[11] V.P. Chumachenko, On the estimation of scattering from convex conducting cylinders, *Microwave Optical Technology Letters* 45 (2005) 191–194.
[12] A.V. Krapyvny, V.P. Chumachenko, On the estimation of scattering from convex impedance cylinders, *Proceedings of the 11th International Conference on Mathematical Methods in Electromagnetic Theory*, Kharkiv, Ukraine, June 26–29, 2006, pp. 248–250.
[13] M. Abramowitz, I.A. Stegun, *Handbook of Mathematical Functions*, Dover, New York, 1972.